Unbinding of Oxidized Cytochrome *c* from Photosynthetic Reaction Center of *Rhodobacter sphaeroides* Is the Bottleneck of Fast Turnover[†]

László Gerencsér, Gábor Laczkó, and Péter Maróti*

Department of Biophysics, University of Szeged, Egyetem utca 2, Szeged, Hungary H-6722

Received July 7, 1999; Revised Manuscript Received September 28, 1999

ABSTRACT: To understand the details of rate limitation of turnover of the photosynthetic reaction center, photooxidation of horse heart cytochrome *c* by reaction center from *Rhodobacter spheroides* in detergent dispersion has been examined by intense continuous illumination under a wide variety of conditions of cytochrome concentration, ionic strength, viscosity, temperature, light intensity, and pH. The observed steady-state turnover rate of the cytochrome was not light intensity limited. In accordance with recent findings [Larson, J. W., Wells, T. A., and Wraight, C. A. (1998) *Biophys. J. 74* (2), A76], the turnover rate increased with increasing bulk ionic strength in the range of 0−40 mM NaCl from 1000 up to 2300 s^{-1} and then decreased at high ionic strength under conditions of excess cytochrome and ubiquinone and a photochemical rate constant of 4500 s^{-1}. Furthermore, we found the following: (i) The contribution of donor (cytochrome *c*) and acceptor (ubiquinone) sides as well as the binding of reduced and the release of oxidized cytochrome *c* could be separated in the observed kinetics. At neutral and acidic pH (when the proton transfer is not rate limiting) and at low or moderate ionic strength, the turnover rate of the reaction center was limited primarily by the low release rate of the photooxidized cytochrome *c* (product inhibition). At high ionic strength, however, the binding rate of the reduced cytochrome *c* decreased dramatically and became the bottleneck. The observed activation energy of the steady-state turnover rate reflected the changes in limiting mechanisms: 1.5 kcal/mol at 4 mM and 5.7 kcal/mol at 100 mM ionic strength. A similar distinction was observed in the viscosity dependence of the turnover rate: the decrease was steep (η^{-1}) at 40 and 100 mM ionic strengths and moderate ($\eta^{-0.2}$) under low-salt (4 mM) conditions. (ii) The rate of quinone exchange at the acceptor side with excess ubiquinone-30 or ubiquinone-50 was higher than the cytochrome exchange at the donor side and did not limit the observed rate of cytochrome turnover. (iii) Multivalent cations exerted effects not only through ionic strength (screening) but also by direct interaction with surface charge groups (ion-pair production). Heavy metal ion Cd^{2+} bound to the RC with apparent dissociation constant of 14 μM. (iv) A two-state model of collisional interaction between reaction center and cytochrome *c* together with simple electrostatic considerations in the calculation of rate constants was generally sufficient to describe the kinetics of photooxidation of dimer and cytochrome *c*. (v) The pH dependence of cytochrome turnover rate indicated that the steady-state turnover rate of the cytochrome under high light conditions was not determined by the isoelectric point of the reaction center (pI = 6.1) but by the carboxyl residues near the docking site.

Water-soluble cytochrome *c* interacts with several redox-active proteins of aerobic and anaerobic respiration (e.g., cytochrome *c* peroxidase, flavocytochrome b_2, NO_2^- reductase, N_2O reductase, NO reductase, cellobiose oxidase, etc.) and bacterial photosynthesis. The physiological role of cytochrome c_2 in photosynthetic bacteria is well established: it shuttles electrons between the integral membrane proteins of photochemical reaction center (RC)[1] and the ubiquinol-cyt c_2 oxidoreductase (for reviews, see refs *1*−*3*). These small (12−14 kDa) single-heme proteins are located in the aqueous periplasmic phase outside the intracytoplasmic membrane and inside the outer membrane (cell wall) of the bacterium. As mobile electron carriers, they diffuse between the electron-donating and -accepting reaction sites of these membrane redox proteins along the membrane−aqueous interface and through the aqueous solution.

Cytochrome c_2 exports oxidizing equivalents from light-activated RC of purple bacterium *Rhodobacter* (*Rb.*) *sphaeroides*. A routine route to study this action is to expose the RC dissolved in detergent or reconstituted in phospholipid vesicles to a brief and saturating flash of light that turns over the RC just once. The RC−cyt *c* system displays kinetically distinct phases. The fast phase [$t_{1/2} \sim 1$ μs (*4*−*7*)] arises from "proximal" (bound) cytochrome at the time of the flash,

[†] We are grateful for the financial support of the Hungarian Science Foundation (OTKA 17362/95, T30337, and M27903), Foundation of Hungarian Ministry of Education (FKFP 1288 and B-23/1997, FEFA III/1034 and IV/1605, and AMFK 043/98), and NATO (LST.CLG 975754).

* Corresponding author. Fax: 36-62-454-121. E-mail: pmaroti@physx.u-szeged.hu.

[1] Abbreviations: cyt^{3+} and cyt^{2+}, oxidized and reduced cytochrome *c*, respectively; K_D, dissociation constant; LDAO, *N*,*N*′-dimethyl dodecylamine *N*-oxide; 1,2-NQ, 1,2-naphthoquinone; P, bacteriochlorophyll dimer that is the primary electron donor in the reaction center protein; Q_A and Q_B, primary and secondary quinone, respectively; Rb., *Rhodobacter*; RC, reaction center; Triton X-100, polyoxyethylene(10) isooctylphenyl ether; UQ_6, ubiquinone-30; UQ_{10}, ubiquinone-50.

10.1021/bi991563u CCC: $18.00
Published on Web 11/25/1999

and the slower phases [$t_{1/2} > 200$ μs (*8*−*14*); $t_{1/2} \sim 100$ μs (*6*); $t_{1/2} \sim 65$ μs (*15*); and $t_{1/2} \sim 55$ μs (*4*)] are attributed to the "off" (unbound) or "distal" (bound) states that require association or reorientation reactions prior to electron transfer. Measurements on optical linear dichroism (*16, 17*), EPR (*17*), viscosity (*13*), and site-directed (L162) mutant of the RC (*6*) indicated that the proximal and distal bound cytochromes are physically distinct, although some authors did not find evidence for a distal site (*7, 18*−*20*). Although many additional interesting kinetic and thermodynamic details of the electrostatically guided binding process could be revealed by the flash assay, it offered only limited understanding of the dissociation of the complex that is essential for cytochrome exchange. The estimates for dissociation rate arose from model calculations to fit kinetic data [900 s^{-1} (*13*); $\sim 1 \times 10^3$ s^{-1} (*6, 12*); $\sim 1 \times 10^4$ s^{-1} (*17, 21*)] or from indirect double flash experiments. The cyt c^{3+}/cyt c^{2+} exchange time gives the upper limit of the two-flash P^+ assay used to determine the rate of conformational gating related to interquinone electron transfer: if cyt c^{3+}/cyt c^{2+} exchange takes place between flashes, P^+ will be reduced by exchanged cyt c^{2+}. For the exchange time, an estimate of 0.5−0.7 ms was given in RC of *Rb. sphaeroides* (*22*).

A more direct method is offered that is closer to the physiological role of the RC−cyt *c* system (for the organization in whole cells, see ref *23*) if we do not avoid the complications attendant with steady-state analysis. Under conventional (not extremely intense) light activation, the light intensity will determine the turnover rate of the RC (*24, 25*). If, however, high steady-state light intensity and rapid acceptor side turnover are assured, then the binding−unbinding dynamics of cytochrome *c* with RC could be uncovered (*26, 27*).

In this paper, we have further investigated and separated the rate-limiting processes in steady-state cytochrome turnover under high light intensity and excess cytochrome and ubiquinone. It will be shown that the observed rate at low ionic strength is limited by the unbinding of oxidized cytochrome. The influences of different physicochemical factors such as viscosity, temperature, external pH, and the presence of mono-, di-, and trivalent cations (including heavy metals) have also been studied.

MATERIALS AND METHODS

Detergent (LDAO)-solubilized RC protein was isolated from blue-green (carotenoidless) mutant (strain R-26) of photosynthetic bacterium *Rb. sphaeroides* as described earlier (*28*). For alternate detergent (Triton X-100) preparation and to remove excess salt that influences the kinetics, the RC preparation was dialyzed against 1 mM Tris buffer (pH 8.0) and 0.03% Triton X-100 overnight at 4 °C before use. The RC isolated in this way was depleted of secondary quinone as checked by biexponential analysis of the kinetics of charge recombination evoked by single saturating flash, where the slow component indicated the presence of functional Q_B (*29, 30*). The secondary quinone activity was reconstituted by ubiquinones added to the sample in excess from 10 mM stocks dispersed in 30% Triton X-100 (UQ_{10}, Sigma) or solubilized in ethanol (UQ_6, Sigma). The degree of reconstitution was above 90%.

Mammalian (horse heart) cytochrome *c* (Sigma) could be used as an external donor to the oxidized dimer (P^+) of the RC because the mitochondrial cytochrome *c* behaves similarly to cytochrome c_2, the native electron donor to P^+ in *Rb. sphaeroides* (*4, 12, 13*). The actual redox potential was mediated by 10 μM 1,2-NQ and was adjusted by sodium ascorbate to a value that was low enough to reduce the cytochrome *c* but not too low to avoid the reduction of the quinones of the RC. The degree of reduction of the cytochrome *c* was monitored as an increase of the absorption at 550 nm in a spectrophotometer (Unicam UV4). The amount of cytochrome *c* oxidized by the RC was determined using the extinction coefficient difference of $\epsilon_{red} - \epsilon_{ox} = 21.1 \pm 0.4$ mM^{-1} cm^{-1} (*31*). As a small P^+ signal persists at 550 nm, which must be subtracted, and 540 nm is isosbestic for cytochrome *c* oxidation, the 550/540 nm difference of kinetic traces is taken if the accumulation of P^+ as compared to oxidized cytochrome *c* is not negligible (e.g., in the initial phase). The bandwidths of the measuring beams were 2 nm in the visible spectral range and 4 nm at 865 nm. The concentration of the oxidized dimer (P^+) was determined from flash-induced absorption change at 430 or 865 nm before addition of donor using extinction coefficients of 26 and 288 mM^{-1} cm^{-1}, respectively (*28, 29*).

The kinetics of the laser-induced absorption changes was measured with a single beam kinetic spectrophotometer of local design (*26*). The probe light crossed the 3 × 3 mm rectangular quartz cuvette horizontally and was measured with a photomultiplier (EMI 9558) through a Corning 4-96 filter in the visible spectrum and with a photodiode (UDT Sensors, Inc., PIN 10DI) through a 850-nm high-pass filter in the near-infrared spectral range. The actinic illumination was achieved by a fiber coupled laser diode [Opto Power; type OPC-A002-796-FC/150, emission wavelength 796 nm, emission bandwidth (fwhm) < 3 nm, maximum power 1.2 W] controlled by a homemade driver (operating current 1.2 A). The duration of the laser emission (typically 5 ms) was controlled by a digital pulse generator (Híradástechnika, type TR 0360), the rectangularity of its shape was checked by a photodiode connected to an oscilloscope through an amplifier, and the light intensity was measured by a pyroelectric joulemeter (Molectron, model J25) (Figure 1a). The laser light was delivered through fiber optics to the bottom of the cuvette. As the measuring beam was focused on a small area (3 mm × 3 mm), the sample absorbed less than 20% of the exciting light only upon crossing the volume illuminated by the probing light. The cuvette was held in a massive brass block channeled for liquid circulation to control the temperature. The temperature in the cuvette was measured with a thermocouple (TH 3010) coupled to a digital thermometer (Vermer VE 305K) and, unless stated otherwise, was 23 °C. The sample was kept under nitrogen atmosphere. Data were recorded by a digital oscilloscope (Hitachi VC 6025) interfaced with an IBM PC where data analysis and model calculations were carried out using Mathcad 4.0. The kinetic analysis of the absorption transients was performed by using the Levenberg−Marquardt algorithm.

RESULTS

The experiments presented examine the cyt *c* photooxidation kinetics in RC detergent suspension under a wide variety of conditions. The kinetic activation is effected by laser diode illumination of rectangular shape that generates oxidized bacteriochlorophyll dimer in the RC. P^+ serves to

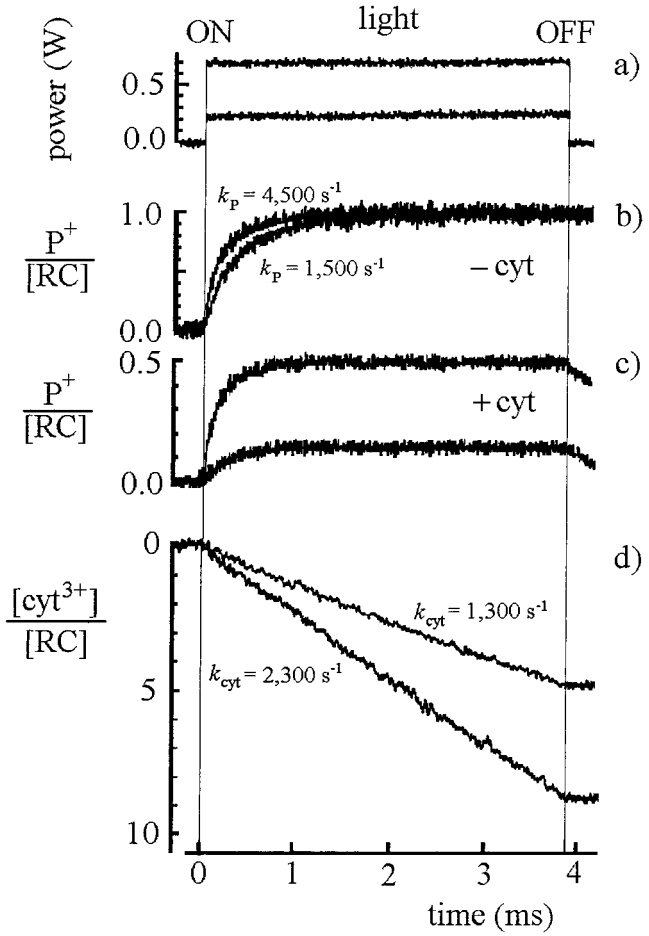

FIGURE 1: Comparative kinetic assays used in this study. Rectangular shape of laser diode emission at 796 nm (a), kinetics of charge separation monitored at 865 nm in the absence (b) and presence (c) of external donor and generation of photooxidized cytochrome relative to RC tracked at 550/540 nm (d). Conditions: 1.0 μM RC, 25 μM UQ_6, 0.03% Triton X-100, pH 5.7, 296 K, 40 mM NaCl, 57 μM cyt^{2+} (c and d) and 10 μM 1,2-NQ (c and d).

oxidize one ferrocytochrome *c*. Once the cyt *c* has transferred an electron to the RC, it dissociates from the RC and is replaced by an other ferrocytochrome *c* from the pool. Thus, the observed rates of photooxidation of P and cyt *c* reflect the molecular dynamics of cytochrome *c* exchange during continuous turnover of the RC.

Figure 1 summarizes all the essential plots used in this study. The time course of the exciting laser diode was rectangular, which significantly simplified the evaluation of the evoked kinetics (Figure 1a). The small illuminated area of the sample assured the detection of homogeneous (not a mixture of different) kinetics but decreased the signal-to-noise ratio of the traces. By the onset of illumination and in the absence of reduced cyt *c*, the simple $PQ \Rightarrow P^+Q^-$ charge separation can be detected as a change in absorbance at 865 nm that is accomplished within a short period of time (Figure 1b). The rate constant of the photochemical reaction, k_P can be determined from the exponential fitting of the trace. The photochemical nature of the reaction is indicated by the linear relationship between the intensity of light excitation and k_P (*26*). In the presence of an external donor, a smaller amount of oxidized dimer is accumulated after a short transient period as a consequence of competition of oxidation by light and re-reduction by reduced cyt *c* (Figure 1c). After turning off the excitation, the decay of P^+ is observed due to cyt re-reduction, which is much faster than the decay controlled by charge recombination ($P^+Q^- \rightarrow PQ$, Figure 1c). In the presence of large reduced cytochrome and quinone pools, photooxidized cytochrome is generated with constant rate through several turnovers of the RC (Figure 1d). In the range of light intensities used here, the rate of cytochrome photooxidation is not proportional to the light intensity: it increases by a factor of only 1.8 (from $k_{cyt} = 1300$ s^{-1} to $k_{cyt} = 2300$ s^{-1}) upon 3 times increase of the light intensity (from $k_P = 1500$ s^{-1} to $k_P = 4500$ s^{-1}). Under our conditions, the observed turnover rate was independent of the type of quinone at the secondary acceptor side as the replacement of UQ_6 (dissolved in ethanol) by UQ_{10} (dissolved in Triton X-100) did not have any effect on the observed kinetics (data not shown).

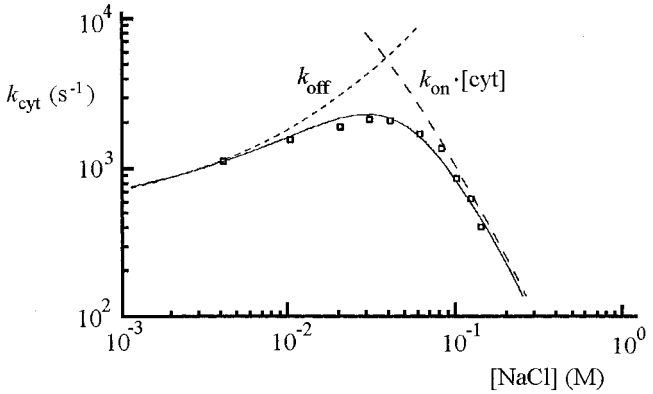

FIGURE 2: Steady-state rate of cytochrome turnover as a function of NaCl concentration of the solution. Conditions were the same as in Figure 1d. The binding (k_{on}[cyt]) and unbinding (k_{off}) rates (dotted lines) and the observed cytochrome turnover rates (solid line) were fit according to the model in Figure 8 with the following parameters: $k_P = 4500$ s^{-1}, $k_{on}(I\rightarrow 0) = 3.8 \times 10^9$ M^{-1} s^{-1}, $k_{off}(I\rightarrow 0) = 4.7 \times 10^2$ s^{-1}, $k_{on}(I\rightarrow\infty) = 6.0 \times 10^3$ M^{-1} s^{-1}, $k_{off}(I\rightarrow\infty) = 5.0 \times 10^6$ s^{-1}, $k_{ox} = 1.0 \times 10^6$ s^{-1}, $R_{RC} = 0.3$ nm, and $R_{cyt} = 0.23$ nm.

Salt Titration. The steady-state turnover rate of cyt oxidation by RC was measured as a function of NaCl concentration of the solution (Figure 2). Contrary to the expectations, the rate was retarded at low ionic strength and accelerated as the salt concentration was increased. At the maximum ([NaCl] = 40 mM), the rate was 2−3 times faster than at limiting low ionic strength. At still higher salt concentrations, the rate of photooxidation declined sharply in good accord with the electrostatic nature of association of RC and cyt observed earlier in single flash experiments. Much above [NaCl] = 100 mM, the cyt does not bind to the RC and the rate of cyt turnover drops below the limit of sensitivity. The direct consequence of this experiment is the existence of a relatively slow (dissociation) process (k_{off}) that is different from association (bimolecular rate constant k_{on}) and limits the rate of cyt turnover in the range of low ionic strength.

Similar behavior was shown by a variety of mono-, di-, and trivalent cations (Figure 3b). For all of the metals tested, the same anion (Cl^-) was used, thus the observed effect on cyt turnover is not caused by the anionic counterion. If the ions had the only effect of ionic screening according to the Debye−Hückel theory, then the curves for different multivalent cations would coincide in the ionic strength (*I*)

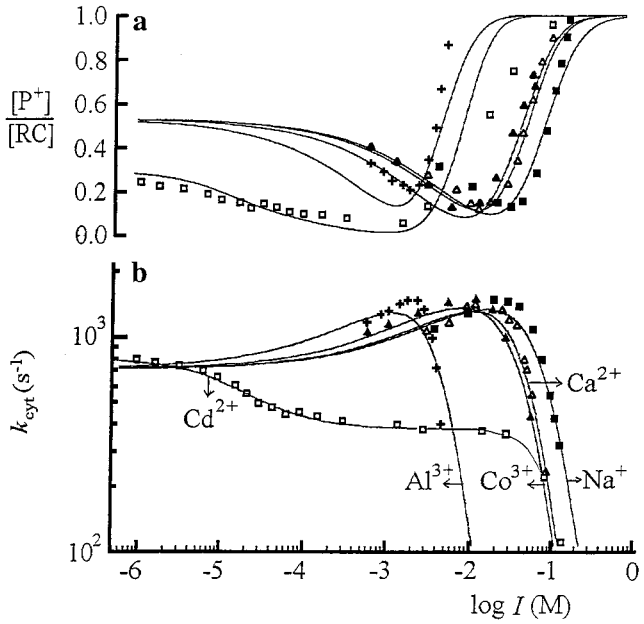

FIGURE 3: Steady-state accumulation of oxidized dimer (a) and steady-state turnover rate of the cytochrome (b) as a function of the ionic strength of added salts: NaCl (■), $CaCl_2$ (△), $[Co(NH_3)_6]Cl_3$ (▲), $AlCl_3$ (+), and $CdCl_2$ (□). Conditions were the same as in Figure 1d except for pH 6.5. The salt-independent fitting parameters were $k_{ox} = 1.0 \times 10^6$ s^{-1}, $k_{on}(I\rightarrow 0) = 3.8 \times 10^9$ M^{-1} s^{-1}, $k_{off}(I\rightarrow 0) = 8.5 \times 10^2$ s^{-1}, $R_{cyt} = 0.23$ nm, and $k_P = 1500$ s^{-1} (except for $CdCl_2$ where a standard dissociation equation

$$k_P = 780\ s^{-1} - \left(1 + \frac{I + K_D}{[RC]} - \sqrt{\left(1 + \frac{I + K_D}{[RC]}\right)^2 - 4 \times \frac{I}{[RC]}}\right) \times 200\ s^{-1}$$

with $K_D = 14$ μM was used). The salt-dependent fitting parameters were

salt	$k_{on}(I\rightarrow\infty)$ (M^{-1} s^{-1})	$k_{off}(I\rightarrow\infty)$ (s^{-1})	R_{RC} (nm)
NaCl	1.5×10^4	4×10^6	0.38
$CaCl_2$	1×10^3	8×10^6	0.38
$[Co(NH_3)_6]Cl_3$	5×10^3	2×10^7	0.53
$AlCl_3$	1×10^1	4×10^7	1.22
$CdCl_2$	1×10^1	4×10^7	1.22

representation. The obvious deviation from the general tendency is the indication of the presence of other effects different from ionic screening. The Ca^{2+} cation is a bit more effective than the monovalent Na^+ ion, the Co^{3+} cation in cobalt hexamine chloride complex $[Co(NH_3)_6]Cl_3$ behaves like Ca^{2+}, but the Al^{3+} cation is much more effective than can be expected from its ionic strength. They all show, however, similar shape with increasing and descending phases as a result of two different rate-limiting steps. The heavy metal ion (Cd^{2+}) has a completely different effect in the range of very low ionic strength as it directly binds to the RC (*32, 33*). The rate limitation in the turnover of cyt below $I \approx 10$ mM is probably caused by the deceleration of proton uptake due to Cd^{2+} binding. At high ionic strength, however, the breakdown of electrostatic guidance (attraction) will limit the rate of turnover as observed in all cases of the cations studied here.

The ionic strength dependence of steady-state level of oxidized dimer was determined too (Figure 3a). The exciting light intensity was high enough to generate P^+ with a rate comparable to that of cyt turnover even at low ionic strength; therefore, a significant amount of P^+ could be monitored. As the steady-state accumulation of P^+ and the rate of photooxidation of cyt are opposing processes, their ionic strength dependence shows reciprocal character: where the rate of cyt turnover is maximal, the P^+ accumulation has its minimum.

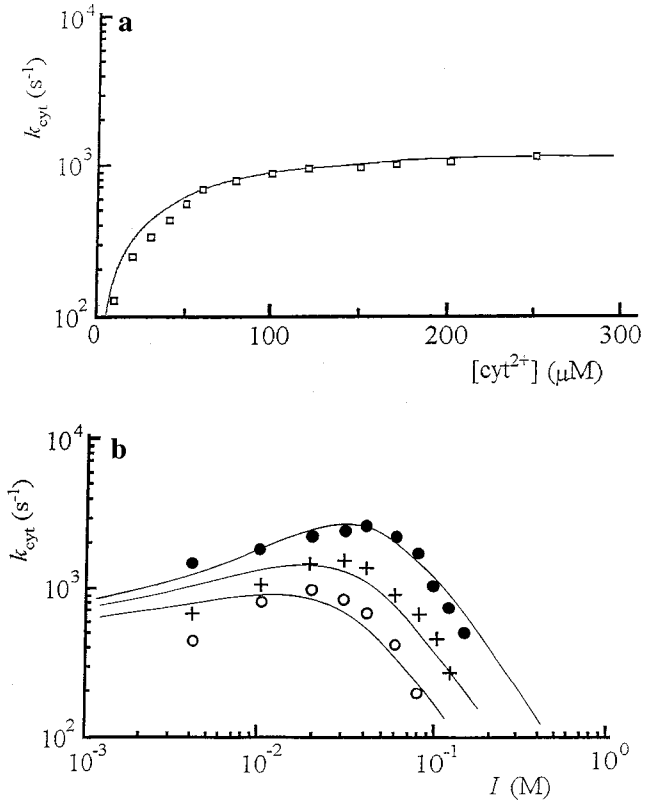

FIGURE 4: Steady-state rate of cytochrome turnover as a function of the pool size of cytochrome (a) and ionic strength of the solution (b) at several fixed cytochrome concentrations. The ionic strength was 100 mM (a), and the concentration of the reduced cytochrome was 57 (●), 18 (+), and 8 μM (○) (b). Otherwise, the conditions were the same as in Figure 1d. The solid curves are fits to the model (Figure 8) taking into account the rebinding of cyt^{3+} to the RC (rate constant k_{on}): $k_{on}(I\rightarrow 0) = 3.8 \times 10^9$ M^{-1} s^{-1}, $k_{on}(I\rightarrow\infty) = 6.0 \times 10^3$ M^{-1} s^{-1}, $k_{off}(I\rightarrow 0) = 470$ s^{-1}, $k_{off}(I\rightarrow\infty) = 2 \times 10^5$ s^{-1}, $k_{ox} = 1.0 \times 10^6$ s^{-1}, $R_{RC} = 0.3$ nm, $R_{cyt} = 0.23$ nm, and $k_P = 1500$ (a) and 4500 s^{-1} (b).

Size of Cytochrome Pool. The steady-state turnover was also measured as a function of the pool size of the reduced cytochrome while all other parameters were kept constant (Figure 4). Even the smallest pool ([cyt^{2+}]/[RC] = 8) was large enough to ensure a stationary phase in the cytochrome turnover kinetics. The salt titration curves of the rates taken under decreasing size of reduced cytochrome pool showed overall drop but preserved their two-phase character: upon increasing ionic strength, the rate of cyt turnover increased moderately but dropped sharply at high ionic strength (Figure 4b). The position of the highest rate shifted slightly toward lower ionic strength: from 40 mM at [cyt^{2+}]/[RC] = 58 to 20 mM at [cyt^{2+}]/[RC] = 8. At small pool size, the observed rate of cytochrome photooxidation was linearly proportional to the cytochrome concentration (pseudo-first-order reaction, Figure 4a). From the initial slope, a bimolecular rate constant of $k_{on} = 1.1 \times 10^7$ M^{-1} s^{-1} can be calculated ($I = 100$ mM). At very large pool ([cyt^{2+}]/[RC] > 100), the observed rate deviates from linearity and tends to saturate.

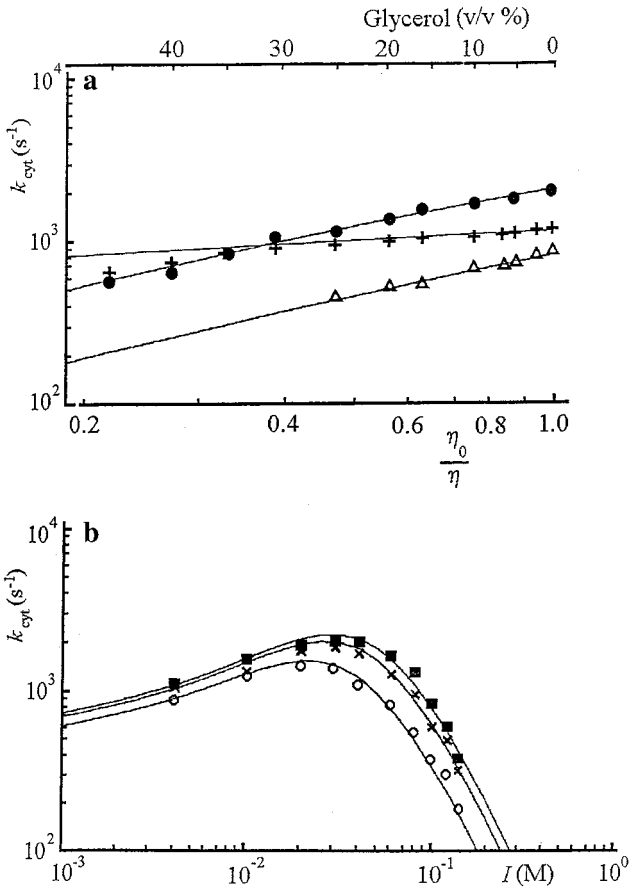

FIGURE 5: Viscosity dependence of steady-state rate of cytochrome turnover: double logarithm plot (a) and salt titration at different viscosities (b). The ionic strength was 4 (+), 40 (●), and 100 mM (△) (a), and the glycerol concentration was 0% (■), 10% (×), and 30% (○) (b). The viscosity of the solution (η) was referred to that of water (η_0). For simulation, the explicit form of the viscosity dependence of the rate constants was $k(\eta) = k(\eta_0)(\eta_0/\eta)^n$ with $n = +1$ for on and $n = +0.2$ for off rates. Otherwise, the conditions and fitting parameters were the same as in Figure 2.

Viscosity Dependence. The viscosity of the solution was adjusted by the addition of glycerol (up to 45% v/v) to the sample. In ionic strength representation, the increase of viscosity decreased the rate of turnover and shifted the steep decline toward lower ionic strength (Figure 5b). This is in good agreement with the diffusion-limited and bimolecular nature of the RC−cyt complex formation, the rate of which is inversely proportional to the viscosity of the solution (Einstein−Smoluchowski equation). The turnover rate changed less at low ionic strengths than at high salt concentrations, indicating that the viscosity dependence of the two phases (dissociation and association) was different. The separation is more straightforward if the turnover rate is plotted as a function of inverse of viscosity in double logarithmic scale for low (5 mM), moderately high (40 mM), and high (100 mM) ionic strengths under conditions where the domination of association is increasing (Figure 5a). The data fit to straight lines with slopes of +0.2 and +1.0.

Arrhenius Plot. In the 275−323 K range, the temperature dependence of the rate of stationary photooxidation of cytochrome *c* was measured with excess cytochrome and ubiquinone at low (4 mM) and high (100 mM) ionic strengths (Figure 6). Over the whole temperature range, single apparent activation energies of 5.7 (at high ionic strength) and 1.5 kcal/mol (at low ionic strength) were determined. The conditions of high and low ionic strengths correspond to the domains where the observed rate is limited by association of reduced cytochrome and dissociation of oxidized cytochrome, respectively. The observed apparent activation energy of 5.7 kcal/mol can be expected for a diffusion-controlled reaction of binding, while much smaller (thermal) energy is necessary to overcome the barrier to separate the reactants.

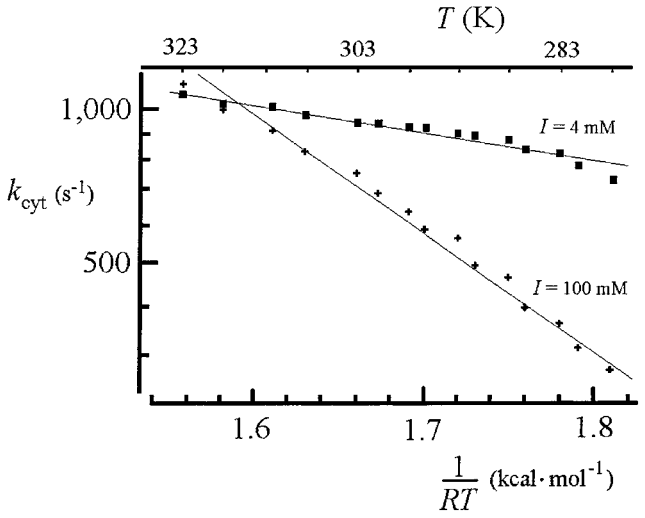

FIGURE 6: Arrhenius plots of steady-state turnover rate of cytochrome at low [I = 4 mM (■)] and high [I = 100 mM (+)] ionic strength. The slopes of the straight lines are 1.5 (■) and 5.7 kcal mol^{-1} (+). Conditions are the same as in Figure 1d.

pH Titration. The shape of salt titration curves do not differ significantly in the neutral and slightly acidic pH range, only a small variation of the rate can be observed (Figure 7b). At constant ionic strength (20 mM), the pH dependence of the turnover rate shows marked changes at the borders (Figure 7a). Above pH 8, there is a sharp drop (not shown) not due to cytochrome limitation but to the dramatic decrease of the proton assisted second electron-transfer rate (*34*). At the acidic limit of the pH range (below pH 5), however, the cytochrome will limit the observed rate. The 7−8 carboxyl groups in the vicinity of the docking site protonate below pH 5; therefore, the RC loses important negative charges that are essential for strong binding between RC and cyt^{2+}. The reduced affinity decreases the rate of cytochrome photooxidation in the acidic pH range dramatically. Considering the pH dependence of the cyt turnover, we can argue that not the global charge of the RC is important [expressed by the isoelectric point, pI ≈ 6.1 (*35*)] but the key protonatable amino acid residues at the docking site.

DISCUSSION

Model and Simulation. We have attempted to fit the observed results using a simple scheme for turnover of the donor side of the RC under continuous illumination (Figure 8). In this simplified model, only the parameters influencing the steady-state rate of the turnover were taken into account. Naturally, the true reaction scheme is more complicated than a simple reversible complex formation with subsequent very fast electron transfer. The monomolecular rate constant of reorientation of the docked complex from distal to proximal state is an order of magnitude larger [$\sim 10^4$ s^{-1} (*4, 6, 15*)]

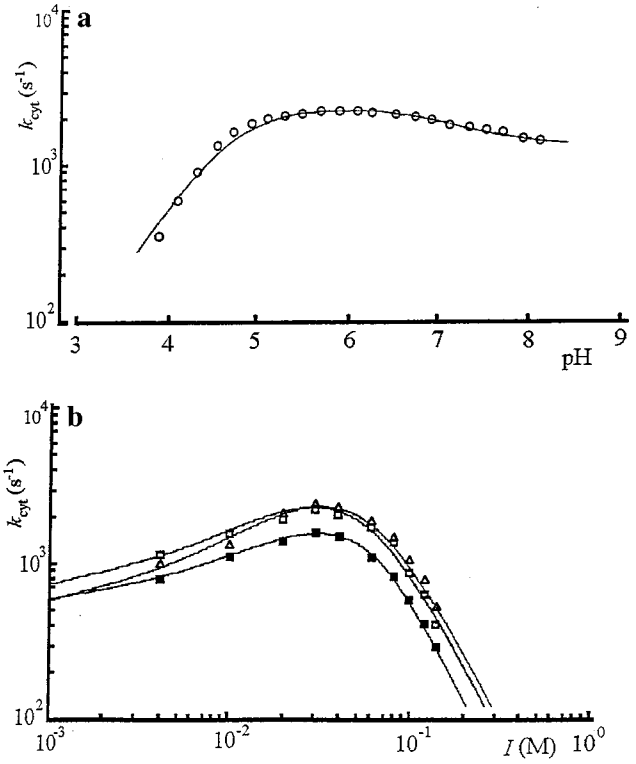

FIGURE 7: Steady-state turnover rate of cytochrome as a function of pH (a, $I = 20$ mM) and ionic strength at pH 5.7 (□), 6.3 (△), and 7.4 (■) (b). Conditions and fitting parameters were the same as in Figure 2, except for $k_{off}(I\rightarrow 0) = 470\ s^{-1}$ (□), $k_{off}(I\rightarrow 0) = 350\ s^{-1}$ (△), and $k_{off}(I\rightarrow 0) = 420\ s^{-1}$ (■); $k_{off}(I\rightarrow\infty) = 5 \times 10^6\ s^{-1}$ (□), $k_{off}(I\rightarrow\infty) = 1 \times 10^7\ s^{-1}$ (△), and $k_{off}(I\rightarrow\infty) = 5 \times 10^5\ s^{-1}$ (■); $k_{on}(I\rightarrow\infty) = 6 \times 10^3\ M^{-1}\ s^{-1}$ (□), $k_{on}(I\rightarrow\infty) = 9 \times 10^3\ M^{-1}\ s^{-1}$ (△), and $k_{on}(I\rightarrow\infty) = 2 \times 10^3\ M^{-1}\ s^{-1}$ (■) (b). The solid curve (a) is a fit to a Henderson−Hasselbalch-type proton dissociation equation with pK values of 4.9 [$k_{on}(pH\rightarrow\infty) = 1 \times 10^8\ M^{-1}\ s^{-1}$ and $k_{on}(pH\rightarrow 0) = 0.0\ M^{-1}\ s^{-1}$] and 6.6 [$k_{off}(pH\rightarrow\infty) = 2.2 \times 10^3\ s^{-1}$ and $k_{off}(pH\rightarrow 0) = 9 \times 10^3\ s^{-1}$].

than that of the dissociation of the complex [$\sim 10^3\ s^{-1}$ (*6*, *13*) and see also Figures 2−5]. Thus, the reorientation represents the rate-limiting step between docking and electron transfer only but not in continuous turnover of the cytochrome. This allowed the use of a two-state model (*18*, *36*) in our calculations instead of the more common three-state model (*8*, *9*, *12*, *13*). The basic assumptions of our model with relevant references to the earlier data are summarized below.

(a) Cyt^{2+} is either free or bound to the RC. Our experiments could not distinguish between kinetically competent (proximal) and incompetent (distal) modes of binding.

(b) Cyt^{2+} has a single binding site in good accordance with data from equilibrium dialysis (*37*) and from cyt *c*−RC cocrystals (*38*). It should be noted, however, that from the cytochrome concentration dependence of the cyt oxidation kinetics, Wachtveitl et al. concluded that their reaction scheme was true only for equimolar reaction conditions (*6*). Under the conditions of excess cytochrome, the results of cytochrome titration were consistent with multiple binding sites for cyt on RC with different binding affinities. Similarly, Overfield and Wraight observed a very tight binding site [$K_D < 10^{-8}$ M (*12*)] in addition to the commonly described binding site [$K_D = 4 \times 10^{-7}$ M (*37*)].

(c) The minimum reaction scheme includes a second-order collisional process of association, a first-order intracomplex

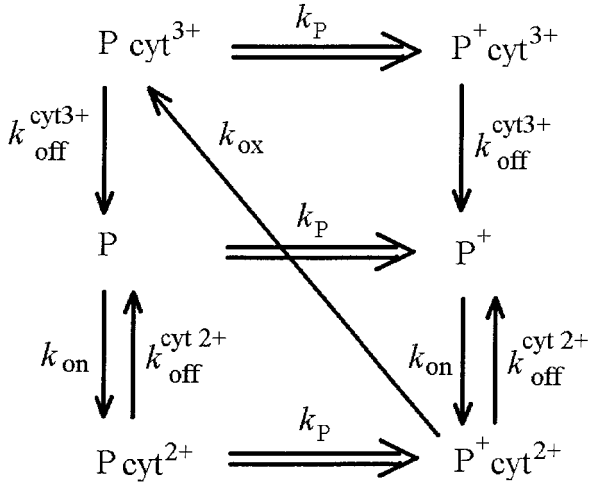

FIGURE 8: Donor site working model of multiple turnover of the RC. The dimer (P) free or bound to cyt can be photooxidized with a photochemical rate constant k_P but can be rereduced only by bound reduced cyt with a rate constant k_{ox}. The cyt^{2+} can associate with RC by a bimolecular collision process with a rate constant k_{on} and dissociate with a monomolecular rate constant k_{off} independently on the oxidation state of the dimer. For reducing the number of fitting parameters, the dissociation rate constants of cyt^{2+} and cyt^{3+} for both states of the dimer were taken to be identical in the calculations. In the case of excess reduced cytochrome ($[cyt^{2+}] \gg [RC]$), the rate of association of the oxidized cyt with RC is much smaller than all other rates; therefore, it is omitted in the scheme. Deceleration of the acceptor side was treated as a decrease of k_P [effects of Cd^{2+} (Figure 3) and low pH (<5) (Figure 7)].

electron transfer, and a first-order reaction for dissociation. The rate constant of $k_{ox} = 1 \times 10^6\ s^{-1}$ (*4*−*7*) was taken for the electron-transfer step (re-reduction of P^+ by bound reduced cytochrome). The rate constants of association (k_{on}) and dissociation (k_{off}) depend on the ionic strengths, viscosity, temperature, and pH of the solution. They are studied separately, and their explicit forms will be given later. At zero ionic strength, the limiting bimolecular rate constant of $3.8 \times 10^9\ M^{-1}\ s^{-1}$ was taken in close agreement with earlier data of $6 \times 10^9\ M^{-1}s^{-1}$ (*10*) and $3 \times 10^9\ M^{-1}s^{-1}$ (*13*) for the diffusion-limited second-order reaction of association. The rate constants of binding and unbinding are controlled by the electrostatic interaction energy (V) between the reactant proteins in opposite way:

$$k_{on}(I) = k_{on}(I\rightarrow\infty)\ \exp\left(-\frac{V}{k_B T}\right)$$

$$k_{off}(I) = k_{off}(I\rightarrow\infty)\ \exp\left(+\frac{V}{k_B T}\right)$$

Here I is the ionic strength of the solution, k_B is the Boltzmann factor, and T is the temperature. Assuming point charges, the interaction energy (expressed in units of kcal/mol) is given by Wherland and Gray (*39*):

$$V = 2.1175 \times \left[\frac{e^{-\kappa R_{RC}}}{1+\kappa R_{cyt}} + \frac{e^{-\kappa R_{cyt}}}{1+\kappa R_{RC}}\right]\left[\frac{Z_{RC}\, Z_{cyt}}{R_{RC}+R_{cyt}}\right]$$

where $\kappa = 3.29/\text{nm}\sqrt{I}$ is the inverse Debye distance, R_{RC} and R_{cyt} are the ion exclusion radii around the charges of charge numbers Z_{RC} and Z_{cyt}, which are taken responsible for the electrostatic interaction between the two proteins. The charge numbers can be expressed by the limiting parameters

for the association:

$$\frac{Z_{RC}Z_{cyt}}{R_{RC}+R_{cyt}}|_{on}=\frac{\ln\frac{k_{on}(I\rightarrow\infty)}{k_{on}(I\rightarrow 0)}}{7.152}$$

and for the dissociation:

$$\frac{Z_{RC}Z_{cyt}}{R_{RC}+R_{cyt}}|_{off}=\frac{\ln\frac{k_{off}(I\rightarrow\infty)}{k_{off}(I\rightarrow 0)}}{7.152}$$

Our model is consistent with virtually all our experimental observations on this system, including the quite different salt, pH, viscosity, temperature, and concentration dependence of the reaction. Solving the differential equations for the scheme and giving appropriate values to the rate constants, either measured directly or approximated based on the equilibrium binding measurements, a set of kinetic curves can be generated. The steady-state turnover rate of cytochrome and the accumulation of oxidized dimer can be calculated yielding the set of fits demonstrated in Figures 2−7. The fitted values in the model are listed in the figure legends. These should be considered as empirical parameters and are not intended to imply any mechanism.

The model readily accounts for the multiphasic nature of the initial kinetics of cytochrome (and dimer) oxidation observed in earlier studies using high-excitation light intensity (*26*). It can be shown that the initial rate is higher than the steady-state rate as cytochromes are already bound to the RC when the laser diode begins to fire (not shown). This observation is in full agreement with single flash experiments that deliver biphasic kinetics for cytochrome oxidation (*4*−*7*).

The cyt^{2+} binding affinity, as given by the dissociation constant ($K_D^{red} = k_{off}/k_{on}$), can be determined at limiting low ionic strength [$K_D^{red} = 0.23$ μM (Figure 3)] and is in good accordance with the earlier data: K_D^{red} has been found to be 0.4 μM in 0.1% Triton X-100 (*37*) and a range of 0.3−10 μM in LDAO with increasing (up to 2%) detergent concentration (*10*, *13*, *37*). In our work, the experimental conditions (excess cyt^{2+} in the initial state) were set to prevent binding of cyt^{3+} to the RC, which would result in a nonfunctional complex. Therefore, no direct data for the dissociation constant of the oxidized cytochrome could be derived from our study. We did not make any distinction in the on and off rates between reduced and oxidized cytochromes. This assumption is supported partly by equilibrium dialysis measurements: the oxidized and reduced forms of cytochrome *c* bind to the RC with approximately equal affinity [$K^{ox}_D = K^{red}_D = 0.35$ μM (*37*)]. Contrary to these results, a 5-fold stronger binding of oxidized cyt *c* relative to reduced cyt *c* ($K^{red}_D/K^{ox}_D = 5$) was concluded from a drop of 40 mV in the redox midpoint potentials of bound and free cytochromes (*13*).

Effect of Cations. The ionic strength dependence of the steady-state rate of turnover showed two distinct phases that we interpret as the manifestation of two rate-limiting steps, namely, the dissociation and the association of active RC−cyt complex (Figure 2). Interestingly, similar ionic strength dependence of the bimolecular rate constant was demonstrated for equimolar concentrations of cytochrome *c* and RC incorporated in negatively charged phosphatidylserine vesicle (*11*). However, the effect was absent in detergent solution or in neutral membranes (*10*). The retarded oxidation rate at low ionic strength was interpreted by the significant electrostatic attraction between the positive cytochrome *c* and the negative surface of the membrane, which could severely limit the rate of diffusion of the cytochrome *c* to the docking site of the RC. Increasing salt concentration diminished the effect by ionic screening.

In our experiments, multivalent cation data were offset in ionic strength representation (Figure 3). The anomalous and widespread effect of multivalent cations on the rate of proton binding (*40*) and on the delayed fluorescence of the dimer (*41*) is well-known and extensively studied. Di- and trivalent cations influence the rate and amplitude of the B_2 phase of transmembrane electric potential in chromatophore at neutral pH to a much greater degree than the monovalent cations (*42*, *43*). At pH 6.2 (close to the isoelectric point of RC), the change of ionic strength by the addition of KCl caused little effect on the B_2 kinetics (*43*). A reversible Ca^{2+}/buffer (imidazole) effect was observed that was explained by a specific interaction of Ca^{2+} ions with carboxyl groups at the RC surface, forming insoluble salts and decreasing the intrinsic buffer capacity of the Q_B site.

Our data imply that the salt effect is not via ionic strength only but through changes in the mobile charge at the protein surface. Heavy metal ions (e.g., Cd^{2+}) directly bind to the RC with high affinity. The steady-state cytochrome turnover assay offered larger dissociation constant ($K_D = 14$ μM at pH 6) than the single flash electron-transfer assay [$K_D = 0.3$ μM at pH 8 (*33*)], and the drop was smaller (about 2 times) in cyt turnover rate than in proton-assisted electron-transfer rate (10 times). This difference could be attributed to different pH values used in these works and to different observed phenomena (rate of proton uptake and cytochrome photooxidation) affected by heavy metal binding to RC.

In our model calculations, small shifts in the ionic dependence of the steady-state rates of cytochrome oxidation could result largely from the change in the dimension of the Stern layer (electrolyte exclusion zone, R_{RC} and R_{cyt}) of the partners. Smaller distances (radii) represent models in which the site of docking is near the point where the heme edge comes nearest to the surface of the protein. In the formation of an activated complex, the degree of access to the heme edge of the cytochrome partially exposed at the surface and the docking site of the RC could be different under various salt conditions. In the salt titration experiments, the ion exclusion radius of the charge on the RC varied between 1.22 nm ($AlCl_3$) and 0.38 nm (NaCl) (Figure 3). Particularly striking examples of mammalian cytochrome *c* oxidation were shown for a variety of substrates of various sizes, charges, and surface properties of inorganic complexes (*39*). In cross-linked RC−cyt c_2 complex, two conformations were identified that differed in the extent to which cyt c_2 had penetrated into the RC surface (*17*). A difference of ∼3 Å in the heme to P^+ distance for the two conformations accounted for a ratio of 80 in electron-transfer rates.

Activation Energy. In the 275−323 K range, Arrhenius behavior is observed with ionic strength-dependent apparent activation energies $E_{a,on}$ and $E_{a,off}$:

$$k_{on}(T) = k_{on}(T\rightarrow\infty)\exp\left(-\frac{E_{a,on}}{RT}\right)$$

$$k_{off}(T) = k_{off}(T\rightarrow\infty)\exp\left(-\frac{E_{a,off}}{RT}\right)$$

where R is the universal gas constant. The activation energy measured at high ionic strength ($E_{a,on} = 5.7$ kcal/mol) shows particular similarity with activation energies of 4.9 (fast phase) and 6.7 kcal/mol (slow phase) for P^+ rereduction by soluble cyt c_2 in isolated RC (*5*). The apparent activation energy at low salt concentrations is significantly lower ($E_{a,off} = 1.5$ kcal/mol) and is remarkably close to that measured in crossed-linked RC−cyt c_2 complex [2.8 (fast phase) and 1.9 kcal/mol (slow phase) (*21*)]. Similarly low activation energy (1.6−2.1 kcal/mol) has been measured for electron transfer from the highest potential heme of firmly attached cytochrome subunit to P^+ in *Rhodopseudomonas viridis* RC (*44*, *45*).

The cytochrome turnover consists of several steps that cannot be easily distinguished based on thermodynamic considerations. The observed apparent activation energy should include the activation energies of the participating processes, such as association (diffusion), distal to proximal reorientation, electron donation, and dissociation of the complex. We found significant changes in apparent activation energies at low and high salt concentrations (Figure 6.). The change in ionic strength should not cause dramatic effects in activation energy of diffusion or Marcus-type (intraprotein) electron transfer. We believe that the thermal activation required to distal to proximal reorientation (together with the distribution between the two states) or to dissociation of the complex should be sensitive to external salt conditions and is the dominating term in the steady-state exchange of the cytochrome. The thermodynamic separation of the steps in cytochrome turnover is not so straightforward as the decomposition based on kinetic measurements. The observed apparent activation energy can be associated with penetration of the protecting hydrophobic residues at or near the protein surfaces and the expected overlap of RC−heme *c* redox orbitals.

Cytochrome Titration. For low cyt concentrations, the slower phase of P^+ reduction after a single flash reflects the second-order binding reaction. At high cyt concentrations, some studies showed a first-order limit of 55−75 μs for the halftime (*4*, *6*, *15*); other investigations, however, did not indicate any saturation (*4*, *5*). Using the assay of continuous cyt turnover, we observed a tendency of saturation above a very high cyt−RC ratio (Figure 4).

After oxidation (or binding in a distal configuration that does not allow electron transfer), cyt^{3+} is released and a new binding can occur. At high cytochrome concentrations, the second-order binding process does not limit this reaction; therefore, the apparent first-order rate monitors the off-rate of the complex. It was concluded from flash kinetic measurements that the half-time for the release of the distal cyt c_2 was close to the fastest observed first-order limits (60 μs) of the slower kinetic component (*17*). Our data referring to continuous light regime cannot make a distinction between the unbinding of oxidized cytochrome from an active complex and the release of reduced cytochrome from an inactive complex. The observed steady-state turnover rate depends only on the slowest step, which is the unbinding of oxidized cyt.

The rate of the rebinding of the photooxidized cyt *c* to the RC can be neglected if the concentration of the reduced cyt *c* is large to that of the RC (Figure 8). At small cyt *c* pool, however, the rate of rebinding of cyt^{3+} becomes comparable to the rate of binding of cyt^{2+} from the pool. This will cause the drop of the observed rate of the cyt turnover at low ionic strength and at small cyt^{2+} pool size (Figure 4b). The deviation of the calculated curves from the measured values can be attributed to simplifying assumptions of the simulation: identical on and off rates of the oxidized and reduced species, time-dependent (not homogeneous) distribution of the products, etc.

Viscosity Dependence. The rate-limiting steps in the turnover rate of cyt can be separated based on viscosity measurements. While the diffusion-controlled association (observed at high ionic strength, Figure 5, and see ref *13*) obeys the Einstein−Smoluchowsky relationship:

$$k_{on}(\eta) = k_{on}(\eta_0)\frac{\eta_0}{\eta}$$

The rate of unbinding of the oxidized cyt *c* (observed at low ionic strength) is supposed to be only mildly viscosity dependent:

$$k_{off}(\eta) = k_{off}(\eta_0)\left(\frac{\eta_0}{\eta}\right)^n$$

Here η_0 is the viscosity of water. Indeed, we found a slope of $n = 0.2$ for low ionic strength in contrast to $n = 1.0$ for high salt conditions (Figure 5).

Regarding the internal movement of the RC−cyt complex, deviation from diffusion controlled reaction was observed by Moser and Dutton (*13*). The viscosity dependence was attributed to proximal to distal transition while the opposite change was viscosity independent. They used it as an indication for physical distinction of the distal and proximal functional states in their three-state model. Here, similar deviation from the Einstein−Smoluchowsky relationship is described. In analogy to their experiments, the mild viscosity sensitivity and moderate activation control of the unbinding reaction of the oxidized cyt *c* may involve orientational and energetic aspects of cytochrome release.

In our experiments, glycerol was added to increase the viscosity of the solution slowing down the bimolecular reaction. The decreased on rate increases the dissociation constant, K_D ($= k_{off}/k_{on}$) observed recently in 60% glycerol (*5*, *19*). The extent of increase cannot be predicted easily from the decrease of the bimolecular reaction rate as the viscosity may have some (but much weaker) effect on the off rate as well (see Figure 5).

Electrostatic and pH Control of Binding and Unbinding. Low ionic strengths and low detergent concentrations promote the well-known electrostatic association of cyt *c* with RC (*4*). There are opposite charges on the interaction surfaces on the RC (net negative charges from L72E, L155D, L257D, L261D, M88D, M95E, M100E, M173E, M184D, and M292D on the periplasmic domain) and the cytochrome *c* (net positive charges from lysine residues at positions 10, 35, 95, 97, and 103 on the heme face) (Brookhaven Data

Base). The solvent-exposed heme edge of the cytochrome is surrounded by positively charged lysine residues and orients toward the negatively charged amino acid residues on the RC. The highly asymmetric distribution of the lysine residues on the cytochrome surface creates a strong electric dipole across the molecule (~300 D), which preorients the cytochrome before binding. From this distal state (initial docking), the cytochrome needs to reorient to an energetically favorable proximal site (final docking) where the electron transfer can take place.

The dramatic decrease in the rate of turnover at high ionic strength clearly indicates the determining role of the charge complementarity of the two redox partners in this interaction. The local distribution of the partial charges at the docking site of both proteins (*38*) rather than the overall net charge of the proteins is important in determination of the electrostatic control. The isoelectric point of cyt *c* is 10.7 (*46*) whereas that of the RC is 6.1 (*35*). Around pH 6, no dramatic changes could be observed in the rate of turnover, although the overall charges of the reaction partner changed oppositely.

A number of localized electrostatic (*4, 47, 48*) and nonelectrostatic (*6, 7, 49*) interactions contribute to tight binding of cytochrome *c* to RC, and it is not possible to assign a priori the pH dependence of cytochrome turnover rate to protonatable amino acid residues on the cytochrome or the RC. We observed, however, a mild pH dependence of the rate of turnover below pH 8 that was followed by a sharp drop in the acidic pH range (Figure 7). The data were fit using pH-dependent on and off rates:

$$k_{on}(\mathrm{pH}) = \frac{k_{on}(\mathrm{pH}\rightarrow\infty) \times 10^{\mathrm{pH}-\mathrm{p}K_{on}} + k_{on}(\mathrm{pH}=0)}{1 + 10^{\mathrm{pH}-\mathrm{p}K_{on}}}$$

$$k_{off}(\mathrm{pH}) = \frac{k_{off}(\mathrm{pH}\rightarrow\infty) \times 10^{\mathrm{pH}-\mathrm{p}K_{off}} + k_{off}(\mathrm{pH}=0)}{1 + 10^{\mathrm{pH}-\mathrm{p}K_{off}}}$$

with apparent p*K* values of $\mathrm{p}K_{on} = 4.9$ and $\mathrm{p}K_{off} = 6.6$. The existence of $\mathrm{p}K_{on}$ with large changes in limiting rates $k_{on}(\mathrm{pH}=0)$ and $k_{on}(\mathrm{pH}=\infty)$ (see legend of Figure 7) clearly indicates that the deprotonation of glutamic acids and aspartic acids in the docking site of the RC may play a determining role in weakening the productive association between the RC and the reduced cyt.

Product Inhibition. A significant product inhibition by oxidized cytochrome *c* bound to the RC was recognized under single (*13*) and multiple turnover (*27*). The observed inhibition can have different (kinetic and energetic) aspects. In the product inhibition model suggested by Moser and Dutton (*13*), the cyt *c* oxidized by one RC can rapidly dissociate and reassociate with another RC not yet reacted with reduced cyt *c*. At low cyt *c* concentrations, product inhibition took place even after a single flash. They showed by redox titration of the cyt *c* oxidation that the RC had comparable binding affinities for oxidized and reduced cyt *c*. In the present studies, we demonstrated a similar product inhibition model based on slow dissociation of the oxidized cyt *c* from the RC and rebinding of the oxidized cyt *c* to the RC in case of small cyt^{2+} pool size (Figure 4b).

Due to the nonlinear time (t)−distance (x) relation for diffusion (in one dimension: $x^2 = 4Dt$, where D is the diffusion coefficient), the diffusion in solution is very fast over short distances such as the distances between the quinone binding site (Q_B) and the pool of quinones in the membrane or between the docking site of cytochrome and the pool of cytochrome in the periplasm. The electrostatics helps to guide the reduced cytochrome *c* to the docking site but inhibits the fast dissociation of the oxidized cytochrome *c*.

It was shown in the present and earlier studies that, in the range of high light intensities, the rate of continuous turnover of the RC was not proportional any more to the light intensity but exhibited saturation due to the contribution of different limiting processes (*26*). At neutral pH and low ionic strength, the rate of steady-state photooxidation of cytochrome *c* by RC cannot exceed a limit of about $2 \times 10^3\ s^{-1}$, determined mainly by the rate of dissociation of the oxidized form of the cytochrome. However, it is important to note that this upper limiting rate of P^+ reduction does not limit photosynthetic growth of the bacterial cells. The conclusion may be supported by light intensity independent doubling times at illuminations comparable to that used in our model experiments with isolated RCs. Not the rate of P^+ reduction but the generation of transmembrane proton electrochemical potential [~200 s^{-1}, (*50*)] is likely to be the growth-limiting process.

CONCLUSIONS

Appropriate conditions were found to separate the different and overlapping rate limiting steps of cytochrome turnover: light intensity, pH, donor and acceptor sides, electron and proton transfer, cytochrome exchange, and dissociation of oxidized cytochrome. At low ionic strength, at neutral or mildly acidic pH, and under high light of excitation, the bottleneck of cytochrome turnover is the rate of cyt^{3+} dissociation. The kinetic and thermodynamic characteristics of association and dissociation of cyt to RC were determined. In the frame of a simple two-state RC−cyt model with rate constants including electrostatic interaction of the partners, the different types of titration experiments could be interpreted with acceptable accuracy. In addition to screen the partner proteins, the cations (particularly the multivalent cations) of the solution decrease the surface (negative) potential of the proteins by ion-pair formation or inhibit principal electron/proton transfer mechanism by direct binding (of mainly heavy metal ions, e.g., Cd^{2+}) to the RC.

ACKNOWLEDGMENT

We thank Drs. Colin A. Wraight (University of Illinois) and Pierre Sebban (CNRS CGM, Gif-sur-Yvette, France) for helpful discussions.

REFERENCES

1. Dutton, P. L. (1986) *Encycl. Plant Physiol. 19,* 197−237.
2. Tiede, D. M., and Dutton, P. L. (1993) in *The Photosynthetic Reaction Center* (Deisenhofer, J., and Norris, J., Eds.) pp 257−288, Academic Press, New York.
3. Meyer, T. E., and Donohue, T. J. (1995) in *Anoxygenic Photosynthetic Bacteria* (Blankenship, R. E., Madigan, M. T., and Bauer, C. E., Eds.) pp 725−745, Kluwer Academic Publishers, Dordrecht, The Netherlands.
4. Tiede, D. M., Vashishta, A. C., and Gunner, M. R. (1993) *Biochemistry 32,* 4515−4531.
5. Venturoli, G., Mallardi, A., and Mathis, P. (1993) *Biochemistry 32,* 13245−13253.

6. Wachtveil, J., Farchaus, J. W., Mathis, P., and Oesterhelt, D. (1993) *Biochemistry 32*, 10894−10904.
7. Wang, S., Li, X., Williams, J. C., Allen, J. P., and Mathis, P. (1994) *Biochemistry 33*, 8306−8312.
8. Dutton, P. L., and Prince, R. C. (1978) in *The Photosynthetic Bacteria* (Clayton, R. K., and Sistrom, W. R., Eds.) pp 525−570, Plenum Press, New York.
9. Overfield, R. E., Wraight, C. A., and DeVault, D. (1979) *FEBS Lett. 105*, 137−142.
10. Overfield, R. E., and Wraight, C. A. (1980) *Biochemistry 19*, 3322−3327.
11. Overfield, R. E., and Wraight, C. A. (1980) *Biochemistry 19*, 3328−3334.
12. Overfield, R. E., and Wraight, C. A. (1986) *Photosynth. Res. 9*, 167−179.
13. Moser, C. C., and Dutton, P. L. (1988) *Biochemistry 27*, 2450−2461.
14. Witthuhn, V. C., Gao, J., Hong, S., Halls, S., Rott, M. A., Wraight, C. A., Crofts, A. R., and Donohue, T. J. (1997) *Biochemistry 36*, 903−911.
15. Long, J. E., Durham, B., Okamura, M. Y., and Millet, F. (1989) *Biochemistry 28*, 6970−6974.
16. Tiede, D. M. (1987) *Biochemistry 26*, 397−410.
17. Drepper, F., and Mathis, P. (1997) *Biochemistry 36*, 1428−1440.
18. Rosen, D., Okamura, M. Y., and Feher, G. (1979) *Biophys. J. 25*, 204a.
19. Mathis, P. (1994) *Biochim. Biophys. Acta 1187*, 177−180.
20. Lin, X., Williams, J. C., Allen, J. P., and Mathis, P. (1994) *Biochemistry 33*, 13517−13523.
21. Drepper, F., Dorlet, P., and Mathis, P. (1997) *Biochemistry 36*, 1418−1427.
22. Graige, M. S., Feher, G., and Okamura, M. Y. (1998) *Proc. Natl. Acad. Sci. U.S.A. 95*, 11679−11684.
23. Vermeglio, A., Joliot, P., and Joliot, A. (1993) *Biochim. Biophys. Acta 1183*, 352−360.
24. Maróti, P., Osváth, Sz., Tápai, Cs., Hanson, D. K., and Sebban, P. (1995) in *Photosynthesis: from Light to Biosphere* (Mathis, P., Ed.) Vol. I, pp 419−424, Kluwer Academic Publishers, Dordrecht, The Netherlands.
25. Maróti, P., Osváth, Sz., and Tápai, Cs. (1998) in *Landmarks in Photobiology* (Hönigsmann, H., Knobler, R. M., Trautinger, F., and Jori, G., Eds.) pp 72−77, OEMF spa, Milano.
26. Osváth, Sz., and Maróti, P. (1997) *Biophys. J. 73*, 972−982.
27. Larson, J. W., Wells, T. A., and Wraight, C. A. (1998) *Biophys. J. 74* (2), A76.
28. Maróti, P., and Wraight, C. A. (1988) *Biochim. Biophys. Acta 934*, 314−328.
29. Kleinfeld, D., Okamura, M. Y., and Feher, G. (1984) *Biochim. Biophys. Acta 785*, 126−140.
30. Stein, R. R., Castellvi, A. L., Bogacz, J. P., and Wraight, C. A. (1984) *J. Cell Biochem. 24*, 243−259.
31. Van Gelder, B. F., and Slater, E. C. (1962) *Biochim. Biophys. Acta 58*, 593−595.
32. Utschig, L. M., Ohigashi, Y., Thurnauer, M. C., and Tiede, D. M. (1998) *Biochemistry 37*, 8278−8281.
33. Paddock, M. L., Graige, M. S., Feher, G., and Okamura, M. Y. (1999) *Proc. Natl. Acad. Sci. U.S.A. 96*, 6183−6188.
34. Paddock, M. L., Senft, M. E., Graige, M. S., Rongey, S. H., Toranchik, T., Feher, G., and Okamura, M. Y. (1998) *Photosynth. Res. 55*, 281−291.
35. Prince, R. C., Cogdell, R. J., and Crofts, A. R. (1974) *Biochim. Biophys. Acta 347*, 1−13.
36. Rosen, D., Okamura, M. Y., and Feher, G. (1980) *Biochemistry 19*, 5687−5692.
37. Rosen, D., Okamura, M. Y., Abresch, E. C., Valkirs, G. E., and Feher, G. (1983) *Biochemistry 22*, 335−341.
38. Adir, N., Axelrod, H. L., Beroza, P., Isaacson, R. A., Rongey, S. H., Okamura, M. Y., and Feher, G. (1996) *Biochemistry 35*, 2535−2547.
39. Wherland, S., and Gray, H. B. (1976) *Proc. Natl. Acad. Sci. U.S.A. 9*, 2950−2954.
40. Maróti, P., and Wraight, C. A. (1997) *Biophys. J. 73*, 367−381.
41. Turzó, K., Laczkó, G., and Maróti, P. (1998) *Photosynth. Res. 55*, 235−240.
42. Shinkarev, V. P., Drachev, L. A., Mamedov, M. D., Mulkidjanian, A. J., Semenov, A. Y., and Verkhovsky, M. I. (1993) *Biochim. Biophys. Acta 1144*, 285−294.
43. Gopta, O. A., Semenov, A. Y., and Bloch, D. A. (1998) in *Photosynthesis: Mechanisms and Effects* (Garab, G., Ed.) Vol. II, pp 873−876, Kluwer Academic Publishers, Dordrecht, The Netherlands.
44. Ortega, J. M., and Mathis, P. (1992) *FEBS Lett. 301*, 45−48.
45. Ortega, J. M., and Mathis, P. (1993) *Biochemistry 32*, 1141−1151.
46. Theorell, H., and Akesson, A. (1941) *J. Am. Chem. Soc. 63*, 1804−1811.
47. Allen, J. P., Feher, G., Yeates, T. O., Komiya, H., and Rees, D. C. (1987) *Proc. Natl. Acad. Sci. U.S.A. 84*, 6162−6166.
48. Caffrey, M. S., Bartsch, R. G., and Cusanovich, M. A. (1992) *J. Biol. Chem. 267*, 6317−6321.
49. Farchaus, J. W., Wachtveil, J., Mathis, P., and Oesterhelt, D. (1993) *Biochemistry 32*, 10885−10893.
50. Donohue, T. J., McEwan, A. G., vanDoren, S., Crofts, A. R., and Kaplan, S. (1988) *Biochemistry 27*, 1918−1925.

BI991563U